1-1-2011

Estimation of Dairy Particulate Matter Emission Rates by Lidar and Inverse Modeling

C. C. Marchant

K. D. Moore

M. D. Wojcik

R. S. Martin

R. L. Pfeiffer

J. H. Pruger

See next page for additional authors

Estimation of Dairy Particulate Matter Emission Rates by Lidar and Inverse Modeling

C. C. Marchant, K. D. Moore, M. D. Wojcik, R. S. Martin, R. L. Pfeiffer, J. H. Prueger, J. L. Hatfield

Abstract. *Particulate matter (PM) emissions from agricultural operations are an important issue for air quality and human health and a topic of interest to government regulators. PM emission rates from a dairy in the San Joaquin Valley of California were investigated during June 2008. The facility had 1,885 total animals, including 950 milking cows housed in free-stall pens with an open-lot exercise area, and 935 dry cows, steers, bulls, and heifers housed in open lots. Point sensors, including filter-based aerodynamic mass samplers and optical particle counters (OPC), were deployed at select points around the facility to measure optical and aerodynamic particulate concentrations. Simultaneously, vertical PM concentration profiles were measured both upwind and downwind of the facility using lidar. The lidar was calibrated to provide mass concentration information using the OPCs and filter measurements. Emission rates were estimated over this period using both an inverse modeling technique coupled with the filter-based measurements and a mass-balance technique applied to lidar data. Mean emission rates calculated using inverse modeling (±95% confidence interval) were 3.8 (±3.2), 24.8 (±14.5), and 75.9 (±33.2) g d^{-1} AU^{-1} for $PM_{2.5}$, PM_{10}, and TSP, respectively. Mean emissions rates based on lidar data were 1.3 (±0.2), 15.1 (±2.2), and 46.4 (±7.0) g d^{-1} AU^{-1} for $PM_{2.5}$, PM_{10}, and TSP, respectively. The PM_{10} findings are roughly twice as high as those reported from other dairy studies with different climatic conditions and/or housing types, but are of similar magnitude as those from a study with similar conditions, housing, and emission rate calculation technique.*

Keywords. *Aerosols, Air pollution, Dairies, Emission, Estimation, Inverse modeling, Lidar, Optimization, Remote sensing, Sampling.*

Agricultural production facilities are being increasingly investigated for emissions of pollutants into the atmosphere in order to understand their contributions to and effects on local and regional air quality. Under the Clean Air Act, the U.S. Environmental Protection Agency (EPA) has set threshold levels for widespread criteria pollutants considered harmful to public health and the environment, referred to as the National Ambient Air Quality Standards (NAAQS). The NAAQS include particulate matter (PM) as $PM_{2.5}$ and PM_{10}, which are defined nominally as the sum of particles with aerodynamic equivalent diameters $\leq$2.5 and $\leq$10 μm, respectively. Furthermore, several state air quality regulatory agencies, such as the State of California Air Resources Board, have begun to require air pollution permits for agricultural operations that exceed certain sizes. The San Joaquin Valley Air Pollution Control District (SJVAPCD) has required agricultural operations of nearly all sizes to select and implement approved Conservation Management Practices (CMPs) since 2005 in order to meet PM_{10} emissions reductions targeted under the EPA-accepted plan to bring the San Joaquin Valley airshed in California into compliance with ambient PM_{10} levels. The EPA redesignated the airshed as being in compliance with ambient PM_{10} levels in November 2008, but sources must continue to implement measures that helped meet PM_{10} NAAQS, including CMPs, as part of their federally approved maintenance plan.

The accurate quantification of agricultural aerosol emission rates is an important part of the regulation process. To date, PM emission rate and emission factor values for dairies in the U.S. are scarce in published literature. Sources of PM from dairies include: animal activity, handling of feed and manure, combustion, vehicle activities on unpaved roads and areas, and windblown soil, manure, and feed. It is expected that PM emission rates vary with multiple factors, including diet, bedding, type of pen or housing, feed storage and distribution practices, waste cleaning and storage practices, animal age, moisture level of soil or animal bedding, and meteorological conditions. A report by the USDA estimated the PM_{10} emission rate for a dairy to be 1.8 g d^{-1} $animal^{-1}$ (USDA, 2000). This was made by extrapolating the previously reported emission rate from a feedlot, and assuming that a dairy has 20% lower emissions. Schmidt et al. (2002) measured PM_{10} concentrations in a naturally ventilated dairy barn during winter and summer, and calculated emission rates by coupling measured concentrations with ventilation rates estimated based on carbon dioxide exchange rates. Winter average PM_{10} emissions were 1.7 g d^{-1} $animal^{-1}$, and summer average

Submitted for review in October 2010 as manuscript number SE 8883; approved for publication by the Structures & Environment Division of ASABE in July 2011.

The authors are **Christian Cardell Marchant,** Electrical Engineer, **Kori Daryl Moore, ASABE Member,** Environmental Engineer, and **Michael D. Wojcik,** Senior Scientist, Energy Dynamics Laboratory, North Logan, Utah; **Randal Scott Martin, ASABE Member,** Associate Professor, Department of Civil and Environmental Engineering, Utah State University, Logan, Utah; **Richard L. Pfeiffer,** Chemist, **John H. Prueger,** Soil Scientist, and **Jerry L. Hatfield,** Director, USDA-ARS National Laboratory for Agriculture and the Environment, Ames, Iowa. **Corresponding author:** Kori Daryl Moore, Energy Dynamics Laboratory, 1695 North Research Park Way, North Logan, Utah, 84341; phone: 435-797-4227; fax: 435-797-4686; e-mail: kori.moore@energydynamicslab.com.

emissions were 0.3 g d^{-1} $animal^{-1}$. Goodrich et al. (2006) made measurements of total suspended particulate (TSP) concentration using filter-based samplers at a free-stall and open-lot dairy over two summers and then measured the particle size distribution (PSD) of the dust to determine the PM_{10} fraction. An inverse modeling technique was applied to the calculated PM_{10} concentrations, using the Industrial Source Complex Short Term Model (ISCST3, ver. 3) to estimate PM_{10} emission rates of 5.0 g d^{-1} $animal^{-1}$ from the free-stall areas and 15.0 g d^{-1} $animal^{-1}$ from the open-lot areas. Using a similar approach, Martin et al. (2006) measured the dust concentration at a dairy during late fall using filter-based samplers and performed inverse modeling with ISCST3 to estimate emission rates of 2.3 and 9.2 g d^{-1} $animal^{-1}$ for $PM_{2.5}$ and PM_{10}, respectively.

Lidar (light detection and ranging), a remote sensing technique, has also been applied previously to investigating agricultural activities. Cooper et al. (1994) used a Raman lidar capable of measuring spatially coherent water vapor structures in order to investigate the mass-energy exchange between the ground and the atmosphere over the canopy of an orchard. Stoughton et al. (1997) used an elastic lidar to map the dispersion of pesticide applied by an airplane over a section of forest, with both horizontal and vertical lidar scanning patterns. These lidar measurements tracked the drift range of the pesticide plumes and were used to verify the accuracy of two different parametric spray drift models. Holmén et al. (1998, 2001, 2008) demonstrated the use of lidar to augment point sampler measurements of PM concentration of emissions from tillage activities. Lidar returned power was compared with mass concentration values measured by point samplers in order to verify plume height and dispersion coefficients from a parametric model. Hiscox et al. (2008) also demonstrated the use of an elastic lidar to map particulate mass concentration from tillage activities, and compared them with mass concentration measurements from point sensors. Eichinger et al. (2005) used an elastic lidar to estimate heat flux emitted from crop fields by measuring the height and width of the entrainment zone, i.e., the boundary layer between aerosols near the surface of the ground and the cleaner air above. These estimates were input into a boundary layer model, which generated an estimate of surface heat flux.

These previous estimates of dairy PM emission rates relied on indirect methods, either by extrapolating values from indirect measurements or by using computer modeling. Scanning aerosol lidar, however, allows direct measurement of aerosol concentration. An investigation of PM emissions from a free-stall and open-lot dairy in the San Joaquin Valley employing CMPs over an eight-day period during June 2008 utilized both direct and indirect emissions measurements and is herein reported.

METHODOLOGY

The PM emission rates from the selected dairy were estimated using two different techniques: an inverse modeling technique with the filter-based samples (Cowherd, 2005) and a flux measurement technique using elastic lidar (Bingham et al., 2009). The PM emission rates were not estimated for the individual potential PM sources within the dairy, but rather an overall PM emission rate was estimated for the entire facility, normalized by the number of animal units in the facility.

SITE DESCRIPTION

The dairy was located near Hanford, California, and was surrounded by agricultural land, including two other dairies located approximately 500 m downwind. The dairy facility is roughly square shaped, covering 22.6 ha, including all associated storage areas and access roads, which are mostly unpaved. It is bordered on its east side by a paved road and on the three other sides by cropland. The total number of animals on the dairy was 1,885, with 950 milking cows, 100 dry milking cows, 30 bulls, 5 steers, and 800 heifers uniformly distributed between birth and two years old. One animal unit (AU) is defined herein as one heifer, steer, or bull cattle and 0.7 milking or dry cattle, according to the U.S. EPA definition (EPA, 2008), totaling 2,335 AU on the dairy. The youngest calves were housed in individual small pens, each with a shelter. Bulls, steers, dry cows, and heifers older than about four weeks were housed in open-lot pens, most of which were equipped with an open shelter. Milking cows were housed in a combination of open-lot and covered free-stall pens. Pens had a total area of 13.7 ha, about 65% of the total dairy footprint. Feed lanes were concrete and sloped for drainage; all other surfaces were unpaved.

The SJVAPCD-accepted CMP plan for this dairy operation addressed the following: feed cultivation, harvest, and storage; unpaved roads and unpaved vehicle/equipment areas for crops; unpaved roads and unpaved vehicle/equipment areas for animal feeding operations; and dairy. For the feed cultivation, harvest, and storage categories, all implemented CMPs pertained solely to crop land and have no impact on PM emissions from the dairy area; this was also the case with the unpaved roads and unpaved vehicle/equipment areas for crops category. The unpaved roads and unpaved vehicle/equipment areas for animal feeding operations category listed the following CMPs: (1) water shall be applied to 1.4 km of private roads, (2) 0.2 km of private roads shall be paved, (3) an 8 km h^{-1} speed limit shall be placed on 1.4 km of private roads, (4) water shall be applied to 0.2 ha of private vehicle/equipment traffic areas, and (5) a 8 km h^{-1} speed limit shall be placed on 0.2 ha of private vehicle/equipment traffic areas. The listed CMPs for the dairy category were the following, with the first three dealing with corral/manure handling and the last two dealing with overall management/feeding: (1) manure from open corrals shall be frequently scraped and/or removed, (2) pull-type manure harvesting equipment shall be used, (3) shaded areas shall be provided for cattle in open corrals, (4) wet material shall be placed in the feed wagon prior to mixing, and (5) feed shall be wetted during mixing. Each implemented CMP is targeted to reduce PM_{10} emissions from the dairy.

The cows were milked twice a day, with a milking schedule from 8:00 a.m. to 5:00 p.m. and from 8:00 p.m. to 5:00 a.m. local time. A feed truck delivered feed to all pens from 5:30 a.m. to 12:00 p.m. and from 3:00 p.m. to 5:00 p.m. local time. Milk cow lanes were flushed with water several times daily, while heifer, dry cow, bull, and steer lanes were scraped approximately weekly. Corrals were scraped as needed, with gathered material stored as a mound in each pen for later removal. No corral scraping occurred during the measurement campaign, although scraping was performed during equipment setup.

SETUP

Historical measurements of wind velocity and direction for the previous three years were obtained from station 15 of the California Irrigation Management and Information System near Stratford, California, 24 km southwest of Hanford. These records showed that wind conditions during the months of May and June were very consistent, with winds coming dominantly from the northwest. Based on these data, instruments were deployed to measure background concentrations northwest of the facility and to measure emission plumes south of the dairy. It was expected that some emission plumes would pass southeast of the facility, but building placement and a lack of permission from neighboring property owners made it impossible to place point sensors at these locations. On-site measurements of the wind direction during the experiment confirmed the dominant direction to be from the northwest. An air quality instrumentation trailer (dimensions approximately 5 m × 2.5 m × 2.5 m) at location AQ in figure 1 was used for the following: sample preparation, collection, and storage; instrument handling, storage, and servicing; and data storage. The lidar instrument (Aglite) was housed within a trailer that was placed approximately 800 m west of the southwest corner of the dairy.

Two 15.3 m towers dedicated to holding meteorological instruments were erected at the site. One was located 400 m west of the dairy, and the other was located just inside the southern boundary of the dairy. Each tower was equipped with five Gill 3-cup anemometers (R.M. Young Co., Traverse City, Mich.; threshold speed 0.5 m s^{-1}, accuracy ±0.2 m s^{-1} over 1 m s^{-1}) mounted at heights of 2.5, 3.9, 6.2, 9.7, and 15.3 m. Five temperature and relative humidity (RH) sensors (model HMP45C, Vaisala, Oulu, Finland; ±0.2°C accuracy at 20°C; RH accuracy of ±2% for values in the range 0% to 90% and ±3% for values in the range 90% to 100%) were also mounted at heights of 1.5, 2.5, 3.9, 6.2, and 9.7 m. Wind vanes (model 024A; Met One Instruments, Grants Pass, Ore.; ±5° accuracy) were mounted on top of both towers at 15.3 m. Campbell Scientific dataloggers were used to record and store the data from the towers. Solar radiation was measured with a weather station (Vantage Pro2 Plus, Davis Instruments, Hayward, Cal.; accuracy ±5% of full scale), which also recorded precipitation (accuracy ±3% or 0.02 mm per event, whichever is greater), temperature (accuracy ±0.5°C for values greater than -7°C, ±1.0°C for values less than -7°C), relative humidity (accuracy ±3% for values 0% to 90% and ±4% for values 90% to 100%), wind speed (±1 m s^{-1} or 5%, whichever is greater), and direction (accuracy ±3°). The Davis Instruments weather station recorded 5 min averages, and the values from the tower instruments were recorded as 1 min averages.

A total of 24 MiniVol PM filter-based samplers (Airmetrics, Eugene, Ore.) were deployed in groups of either two or three instruments at multiple locations around the dairy in order to allow characterization of the particle mass distributions ($PM_{2.5}$, PM_{10}, and TSP) of both background and emitted aerosols. The MiniVol is a portable, programmable, filter-based sampler that yields mass concentration averaged over the sample time, with an impactor plate assembly employed for a single-sized particle fractionation. A pair of samplers consisted of one PM_{10} sampler and one $PM_{2.5}$ sampler, whereas a group of three samplers consisted of one TSP sampler, one PM_{10} sampler, and one $PM_{2.5}$ sampler.

The 47 mm Teflon filters of the MiniVol samplers were pre- and post-conditioned according to the protocols outlined in 40 CFR 50 Appendix J (EPA, 1987). Final average filter weights for both pre- and post-test were calculated from three stable weights within ±5 μg determined using a microbalance (Type MT5, Mettler-Toledo, Inc., Columbus, Ohio). Balance accuracy was verified every ten filter measurements using a 1.000 mg calibration weight. Mass collection was determined by subtracting the pre-weight from the post-weight. Mass concentration was then calculated by dividing the mass collected by the total volume of air sampled, which is the product of the sample flow rate and sample time.

We followed the EPA standard definitions of $PM_{2.5}$ and PM_{10} (EPA, 2004, 2006), under which the measurement efficiencies of the $PM_{2.5}$ and PM_{10} samplers are not perfect step functions with respect to particle size. Instead, there is a slope associated with the removal efficiency of the separation mechanism that leads to removal of some particles smaller than the target size and throughput of some particles larger than the target size. As a result, the measured PM values do not correspond perfectly with a step-function definition of PM concentration. The aspiration efficiency of MiniVol samplers has not been quantified in peer-reviewed literature. However, several studies have compared TSP, PM_{10}, and $PM_{2.5}$ MiniVol measurements with FRM and other high-volume samplers; these studies have found that MiniVol samplers yield results between 0% and 20% lower than high-volume samplers (Baldauf et al., 2001; Chen et al, 2007; Chow et al., 2002). Thus, our measured concentrations and estimated emission rates may be considered as conservative values for this facility.

Nine aerosol profilers (model 9722, Met One Instruments, Inc.), also known as optical particle counters (OPCs), were co-located with several of the sampler groups. The OPCs measured the optical particle size distribution with a period of 20 s using eight discrete size bins, counting the number of particles with diameters between two sequential cutoff values. The lower bin values were 0.3, 0.5, 0.6, 1.0, 2.0, 2.5, 5.0, and 10.0 μm, with the eighth bin measuring all particles whose diameter was greater than 10 μm. Flow calibration of the MiniVols was carried out just prior to the study, and the OPC flow measurements were conducted prior to and after the study, as well as counting calibrations and comparisons between all OPCs. As with the MiniVols, the OPCs also give conservative numbers because particles larger than about 25 μm have difficulty entering the inlet and return such a large optical signal that they are not recognized as valid measurements. Furthermore, at wind speeds >3 m s^{-1}, particles as small as 5 μm may have difficulty entering the instrument inlet (R. Falbo, Met One Instruments, Grants Pass, Ore., personal communication, February 2011).

The PM sampling layout during the field campaign is shown in figure 1. The locations of instrumentation towers are illustrated using solid black symbols, including the location of the Aglite lidar instrument in the bottom-left corner of the figure. The dotted lines extending from the Aglite instrument represent the beam paths of the vertical profile scans. The dairy footprint is shown by a gray rectangle, and within it the pen, free-stall, and manure storage areas of the dairy are represented by white polygons. The expected dominant wind direction is shown by an arrow in the top-left corner.

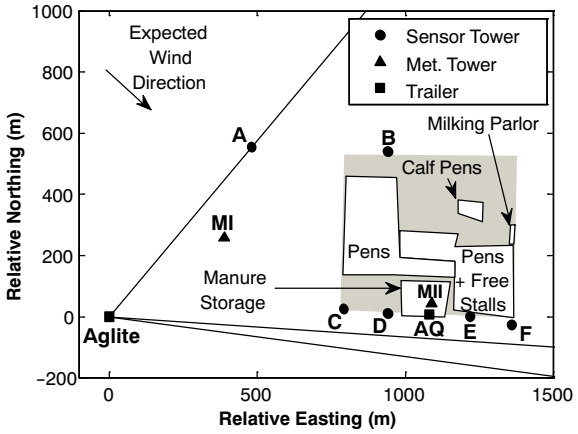

Figure 1. Map of dairy footprint, pens, manure storage, and sampling locations.

Upwind/background point sampler groups were located to the northwest (A) and north (B) of the dairy at 2 and 9 m elevations, respectively. Downwind measurements were made along the southern edge of the dairy at locations C (9 m), D (2 m), E (2 m), F (2 m), and AQ (2, 5, and 9 m), with sampler heights above ground level shown in parentheses. At the AQ location, the instruments at 5 m height were mounted to a trailer and the instruments at 2 and 9 m heights were mounted on a tower located 5 m west of the trailer, upwind or crosswind of the trailer during >95% of the sample collection times. Due to their close proximity to the dairy, it was expected that all of the five downwind locations would be impacted by the emission plume at least to some degree, and this assumption was proven true over the course of the campaign.

Samples of the soil on unpaved roads and in dry-lot pens were collected on June 16 and gravimetrically analyzed for percent moisture level. The analysis showed that the average percent moisture $\pm 1\ \sigma$ was 0.56 ± 0.50 ($n = 3$) and 5.3 ± 5.1 ($n = 7$) for the unpaved roads and pens, respectively. We observed that the roads were well compacted and did not appear to have significant loftable material; no quantitative analysis of the road or pen composition was performed.

Inverse Modeling

Sources of PM at the dairy were modeled using the American Meteorological Society and U.S. Environmental Protection Agency Regulatory Model (AERMOD) software, version 07026 executable file. The interface used to run this model was the commercially available AERMOD View package by Lakes Environmental, Inc. (Waterloo, Ontario, Canada). The model assumes steady-state conditions, continuous emissions, and conservation of mass. It requires that the source type, size, location, and emission rate be specified, as well as sampler or receptor locations. It also requires hourly averaged meteorological data, including wind speed, wind direction, temperature, and solar radiation. The wind speed and direction data were taken from the instruments mounted at 6.2 m, and temperature data were taken at 2.0 m height at location MII in figure 1. Incoming solar radiation values from the Davis Instruments weather station were used in producing the surface meteorological file for AERMOD. Cloud cover was set to be zero for the entire period, as there were clear skies throughout the measurement campaign.

The AERMOD meteorological preprocessor AERMET requires assumptions about the Bowen ratio, noon-time albedo, and surface roughness length, which were chosen as follows: a Bowen ratio value of 1.0, the spring-time default under dry conditions for cultivated land; a noon-time albedo value of 0.18 based on the value given for light-colored, dry soil by Hansen (1993); and a surface roughness length value of 0.10 m, assuming that the dairy layout and structure produced a surface roughness length near the middle of the values given for all agricultural crops (0.04 to 0.20 m) as reported by Oke (1987) and the default AERMET values (0.03 to 0.20 m).

Specific areas of the dairy were modeled as sources of PM emission, including the pens of the heifers, dry and lactating cows, bulls and steers (13.3 ha), as well as calf hutches (0.4 ha), totaling 65% of the dairy footprint. These are marked in figure 1 as calf pens, pens, and free stalls. The free-stall and open-lot pen areas were intermixed, meaning that there was no practical way to differentiate between their effects on the total emission rate of the facility. For this reason, one emission rate was used for all areas. The effects of the air quality instrumentation trailer (AQ) on dispersion and nearby concentrations could not be modeled within AERMOD because the software does not allow the modeling of building effects with area sources. Fugitive dust emissions were seen during the campaign due to vehicle traffic on the unpaved service roads; however, these emissions were intermittent and not modeled but were instead attributed to pen emissions as part of the operational activities of the dairy. Fugitive dust emissions were witnessed from brief tractor activity immediately south and downwind of the facility and of the measurement locations on June 13. The OPC data from the time of the activity were inspected, and no discernable impact was observed. No other potential external sources of aerosol were observed. In addition, it was assumed that PM emissions from the wastewater lagoon and solids separator basin were negligible compared to other sources.

The models require *a priori* values for the emission rate, which is the very value that we seek to derive, in order to predict the PM concentration values, which we have already measured. Inverse modeling is the process of adjusting the model emission rate and comparing the model-predicted concentrations to the already-measured concentration values until a least-squares fit is found of the predicted concentration values to the measured values. The model emission rate that corresponds to that least-squares fit is the inverse modeling estimate.

AERMOD only predicts concentrations resulting from specified sources, in this case the dairy pens, so background/upwind PM levels must be subtracted from concentrations measured downwind of the dairy for comparison in inverse modeling. Facility-produced PM concentrations, or concentrations resulting from the dairy activities, were calculated on a location-by-location basis by subtracting the average upwind concentration from the measured downwind concentration. This difference was determined to be significant if greater than the 67% confidence interval about the upwind measurements, corresponding to one standard deviation. Only facility-produced concentrations deemed significant were used in inverse modeling.

An initial or "seed" emission rate for a given sampling period was chosen and fed into AERMOD, resulting in an initial set of predicted concentration values, which were assembled into a vector. A linear relationship between the emission rate and the predicted concentration was calculated as:

$$\mathbf{pm}_0 = \mathbf{c}e_0 \quad (1)$$

where e_0 is the initial emission rate, $\mathbf{pm}_0$ is the corresponding vector of predicted concentration values from AERMOD, and $\mathbf{c}$ is a vector of coefficients that relate e_0 and $\mathbf{pm}_0$. The measured concentration values from the same sampling period were assembled into another vector, $\mathbf{pm}_{meas}$. The optimal emission rate was calculated to be the minimum least-squares estimate of $\mathbf{pm}_{meas}$:

$$e = \frac{\mathbf{c}^T \mathbf{pm}_{meas}}{\mathbf{c}^T \mathbf{c}} \quad (2)$$

The calculated value of e was input into AERMOD, as well as the values $e \pm 0.01$ g d^{-1} animal^{-1}, and e was confirmed to be the minimum mean-squared solution. This procedure was performed for each sampling period, resulting in individual estimated emission rates.

Elastic Lidar

Elastic lidar is a remote sensing technology with an application in imaging aerosols in the atmosphere (Measures, 1984). Lidar (also known as laser-radar) functions by emitting a pulse of laser light and measuring the intensity and timing of the light as it is scattered by molecules and aerosols in the atmosphere. By recording the direction of the laser beam, as well as the timing and intensity of the scattered light, it is possible to construct an image of the aerosol in the atmosphere. The ability of elastic lidar to directly map aerosol concentration in the atmosphere enables measurement of aerosol emission rates with higher temporal resolution than through inverse modeling. In addition, elastic lidar enables measurement of aerosol concentration at thousands of points at relatively high temporal and spatial resolution, in contrast to a handful of filter samplers, which only measure aerosol concentration at a single point averaged over a time period typically measured in hours to days.

Aglite is an elastic lidar instrument that was used to measure PM emissions at this dairy. Aglite is a three-wavelength micro-pulse scanning lidar, capable of imaging a 400 m high aerosol profile of the atmosphere in 25 s, with 8 m vertical resolution, 6 m horizontal resolution, and single-photon measurement precision (Marchant et al., 2009). It requires data from both the OPCs and filter samplers for calibration and conversion of optical data into mass concentrations. The measured accuracy of Aglite can be described using the 95% confidence interval of PM_{10} concentration measurements. During previous campaigns, this has been shown to have values between 10% and 50% of the mean background concentration and depends on several factors, including the level of atmospheric aerosol loading and the distance of the measurement from the lidar (Zavyalov et al., 2009). The 95% confidence interval at 730 m (the range to the calibration OPC) was approximately 30% of the background PM_{10} concentration, or 10 μg m^{-3}, on average over the course of the campaign. The Aglite instrument was regularly calibrated approximately every 10 min throughout each day by co-locating its scanning beam next to a cluster of point sensors, which was mounted on a tower upwind of the dairy. The OPC in the cluster provided measurements of the shape and magnitude of the optical PSD of the background atmosphere with a 20 s sample period. Additionally, OPCs were located downwind of the dairy and measured the optical PSD of the impacted atmosphere. By taking the difference between upwind and downwind OPC data, the PSD of the emission plume was calculated. Figure 2 outlines the general operation of the Aglite data processing algorithm and illustrates the dependence of the different steps of the algorithm on point sensor data.

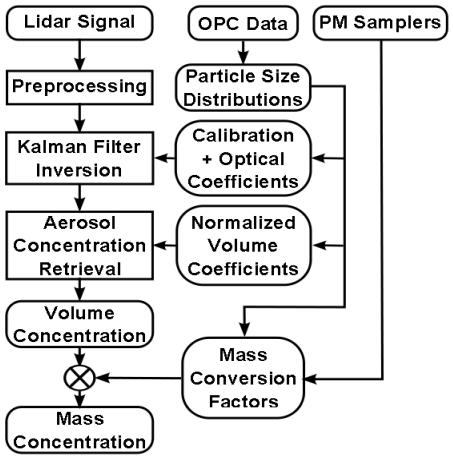

Figure 2. Flowchart outlining the general operation of the Aglite algorithm for converting measured power into PM mass concentration.

The PSDs of background and emission aerosols are measured by OPCs, to which Mie scattering theory is applied in order to calculate optical backscatter and extinction coefficients. Index of refraction values for a water-soluble type aerosol from Jursa (1985) were used in this analysis based on the following: limited downwind chemical composition measurements not herein reported showed fine particles strongly dominated by water-soluble aerosol; the assumption that a significant portion of the aerosol emitted from the dairy was organic and water-soluble; and the very small differences given by Jursa (1985) for the indices of refraction for water-soluble type aerosols and mineral-type aerosols. Mineral-type aerosols, i.e., crustal material, was likely another significant portion of the aerosol emitted by the dairy, as found by Lange et al. (2009) downwind of beef cattle feedlots. By aiming Aglite past the upwind OPC, calibration coefficients were calculated to establish the relationship between the optical properties of the atmosphere and photons detected by Aglite (Marchant et al., 2009).

Since both Aglite and the OPCs detect dust optically, in order to estimate the effective volume concentration of an aerosol, it must be assumed that the detected particles are spherical and have the same index of refraction as the calibration aerosol. This effective volume concentration is not necessarily equivalent to the true total volume of the aerosol particles, as the particles may be non-spherical or have a different index of refraction. In addition, a conversion factor is required to convert the lidar volume-concentration measurement to units of mass; this is called the mass conversion factor (MCF) by Zavyalov et al. (2009). It is derived using co-located OPCs and MiniVol samplers. The

OPC volume concentration, defined as the total volume of all particles in a given volume of air (V_{TSP}) or the total volume of those particles whose optical diameter is less than or equal to either 2.5 ($V_{2.5}$) or 10 μm (V_{10}), is averaged over the MiniVol sample time. The MCF is defined as the ratio of the PM concentration measured by a MiniVol sampler over the corresponding volume concentration measured by an OPC. Because it measures the PSD, a single OPC can measure the separate effective volume concentrations corresponding to $PM_{2.5}$, PM_{10}, and TSP. The MCF incorporates into a single coefficient the differences between mass measurement and optical measurement techniques as well as the effects of many aerosol characteristics that are otherwise difficult to accurately measure in ambient air (i.e., particle shape, index of refraction, porosity, and density). Furthermore, the MCF accounts for the imperfect measurement efficiency of the MiniVol samplers. As a result, the MCF allows the OPC-measured volume concentration values to be converted to PM concentration values that are equivalent to what would have been measured by a MiniVol sampler. By extension, lidar data can also be converted to PM concentration values by first converting the data to OPC-equivalent volume concentration, and then multiplying by the MCF, resulting in MiniVol-equivalent PM concentration values.

The OPCs detect aerosol particles by measuring their side-scatter intensity with a 670 nm laser, and they were calibrated using an aerosol of polystyrene spheres of known diameter. Although the sphericity and complex refractive index of the calibration aerosol (1.59 - 0.0005*i*; Ma et al., 2003) differs from the complex refractive index of a water-soluble aerosol (1.53 - 0.007*i*), the OPC output aerosol profile concentrations were used "as is" and no attempt was made to modify them to compensate for this difference. The assumption that the background and emission aerosols have the same refractive index values as a water-soluble type aerosol may result in error if the true refractive index values differ significantly. In future measurement campaigns utilizing optical instruments, *in situ* measurements should be made of the physical composition of the aerosols in order to confirm that appropriate refractive index values are chosen. The use of the MCF is expected to partly compensate for the error in estimated mass concentration due to this difference in refractive index.

The lidar system uses information about the shape of the PSD of the emission aerosol but does not use any information about the concentration of emission aerosol from the downwind point sensors. Again using Mie theory, the optical backscatter and extinction coefficients of the emission plume were calculated from the emission plume PSD, as well as the volume-concentration coefficients. The optical coefficients were assembled into vectors, whose elements corresponded to the wavelengths of the lidar, whereas the elements of the volume-concentration vector corresponded to the different size fractions of PM. All three of these vectors are then normalized by the magnitude of the backscatter vector and are then used by the lidar data processing algorithm.

It was observed that the aerosol PSD seen by the OPCs varied over the several hours of each measurement period, but that it was relatively constant over the brief periods of time between lidar calibrations. For this reason, atmospheric light-scattering coefficients were calculated for each time period between lidar calibrations and applied to processing of lidar data taken during each corresponding 10 min period. As a result, change in the PSD over the course of the sample period did not affect the conversion of lidar data from raw power to volume concentration.

Aerosol volume-concentration values are estimated from the return power measurements of Aglite by a form of the extended Kalman filter (Dias et al., 2004; Marchant et al., 2011). The filter uses the Aglite calibration coefficients and the normalized optical backscatter and extinction coefficients of the emission aerosol, as measured by the OPCs. The atmosphere is approximated as a linear combination of basis aerosols, or in other words, as an external mixture (Hess et al., 1998). For this specific experiment, the atmosphere is approximated as a uniform background aerosol plus a single variable-emission aerosol.

The filter converts measured return power to basis-aerosol amplitude, as illustrated by the vertical profiles in figures 3a and 3b. These graphs show a downwind vertical scan taken at 5:23 p.m. on June 13. For this experiment, the atmospheric aerosol was approximated as a uniform background aerosol plus a single variable-emission aerosol. The normalized volume concentration coefficients and MCF values are then used to convert basis-aerosol amplitude to mass concentration, as shown in figure 3c. The flow rate of PM passing perpendicularly through each square meter of the lidar scan is the aerosol PM flux concentration. This was calculated by multiplying the PM concentration at each point by the perpendicular component of the wind velocity at that height and is illustrated in figure 3d.

Lidar technology can estimate the total PM emission rate from a source using a mass balance technique and a scanning pattern consisting of vertical scans both upwind and downwind of the source. An example of this scan geometry is illustrated in figure 4, which shows PM_{10} vertical concentration profiles both upwind and downwind of the dairy (the same scan as illustrated in fig. 3), as well as a horizontal image of PM_{10} concentration of the atmosphere near the ground over the dairy. The obstructing power lines at 1400 m east can be seen as dark blotches in the horizontal portion of the scan. The configuration of the lidar sampling is also illustrated by the dotted lines in figure 1.

Each lidar scan began with a continuous stare for calibration purposes at 0° elevation and 41° azimuth, clockwise from true north, lasting 40 s and pointing past upwind sample location A. This was followed by two vertical scan pairs upwind of the facility, also at 41° azimuth. The dashed line extending from the Aglite trailer to location A in figure 1 represents the direction of the upwind profile scan and calibration stare. The beam was then horizontally scanned about 10 m over the dairy from the upwind to downwind sampling locations, which was followed by five vertical downwind scan pairs. The vertical scan pairs consisted of one up scan and one down scan, in which the beam began pointing parallel to the ground, was raised to 25° elevation over 25 s, and then lowered back to ground level over 25 s. Three vertical scan pairs were made on the downwind border of the dairy at 90° azimuth, with two more at different distances downwind of the dairy at 94° and 98° azimuth. Unfortunately, due to a logistical error, the vertical scans made at 90° azimuth, parallel to the downwind border of the dairy, were impaired by backscatter of laser light off of the guy wires of a downwind instrument tower. For this reason, only the vertical profiles taken at 94° and 98° azimuth were used for estimating aerosol emissions. The two

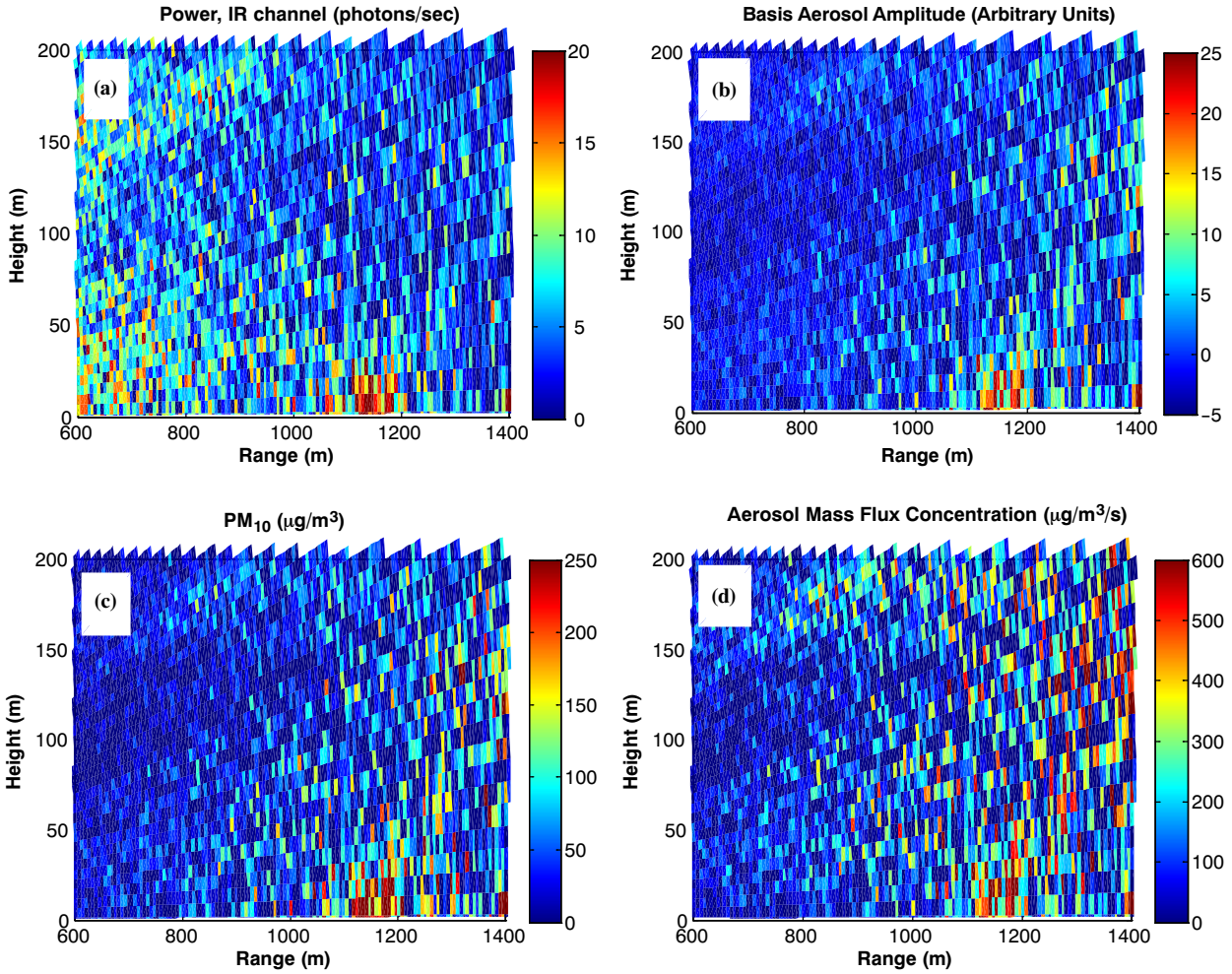

Figure 3. Four sequential data processing steps showing the conversion of (a) raw measured power to (b) basis-aerosol amplitude, (c) PM_{10} mass concentration, and (d) PM_{10} flux concentration.

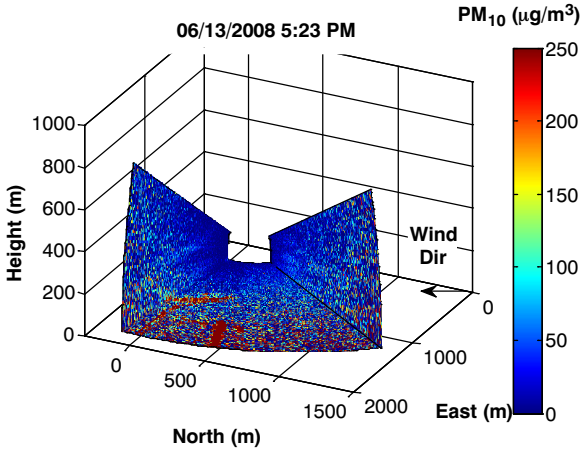

Figure 4. Example of Aglite scan configuration showing upwind and downwind vertical PM_{10} concentration profiles.

dashed lines extending from the Aglite trailer past the south of the dairy in figure 1 represent these two scan angles for profile scans that did not suffer interference from instrument towers. The use of the two separate downwind profile scans was motivated by an attempt to monitor changes in plume morphology at multiple ranges from the emission source, which is not discussed here.

Differences between the upwind and downwind scans were then converted into individual measurements of the flux of aerosols through the downwind scanning plane of the lidar, which is the dairy aerosol emission rate, using wind velocity profiles from measurements collected at the meteorological towers. In this way, the net emission rate of a facility can be directly observed with high temporal resolution and without requiring a mathematical model of the emission process (Bingham et al., 2009). This net emission rate is generally measured at the facility boundary, not taking into account any falloff in aerosol concentration that may occur as the plume continues downwind. Lidar scans were excluded from the dairy emissions analysis if the wind direction deviated more than $\pm 60^\circ$ from north. Lidar scans were also visually inspected for potential problems, such as aerosol-source activity in the upwind area or returns from solid objects; an observed example of a solid object returning the laser signal is a sampling tower or its guy wires.

Measurements

The measurement campaign began at noon Pacific Standard Time (PST) on June 13, 2008, and lasted through midnight on June 20, 2008. All stated times are in PST. For logistical reasons, the OPC and MiniVol instruments were not

available to make measurements on the afternoon of June 18 and all of June 19. The lidar was operated continuously until it was stopped at 19:30 on June 19 due to a malfunction of its laser. One more period of measurements was conducted with the OPC and MiniVol instruments on June 20. Meteorological conditions throughout the field study were hot and dry, with diurnally consistent winds. The mean temperature of the seven measurement periods at 10 m height was 28.8°C; cloud cover was absent or extremely light and at high altitudes throughout, with no recorded precipitation events. Calm or very low wind conditions existed each morning before sunrise with unstable direction. The wind speed at 6.2 m height from 5:00 to 6:00 a.m. varied between 0 and 2 m s^{-1} with a campaign average of 1.2 m s^{-1}. The average wind direction during all sample periods was from the northwest, with an average speed of 2.6 m s^{-1} and a standard deviation of 1.2 m s^{-1} at 6.2 m height.

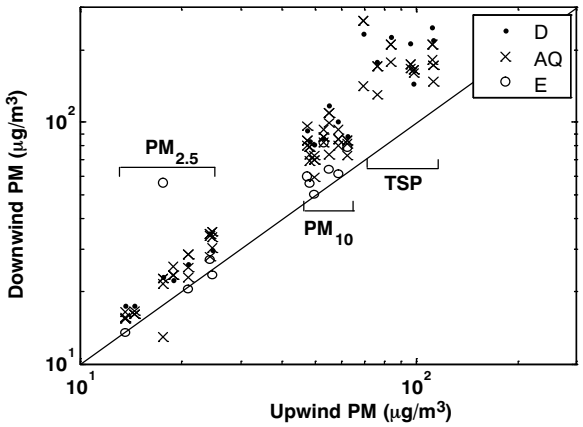

Figure 5. Correlation between upwind (location A) and downwind (locations AQ, D, and E) PM concentrations over all seven sampling periods.

Point Samplers

The filter samplers were run over seven separate periods from June 13 until June 20. On June 13, they ran from noon until 23:00 PST. On June 14, 15, 16, and 17, they ran from 00:30 until 23:00. On June 18, the filters ran from 00:30 until noon, and on June 20 the samplers ran from 11:00 until 23:00. There was a logistical break of 1.5 h between sample periods to allow for instrument inspection, data recording, and placement of fresh filters in the MiniVol samplers.

Measured $PM_{2.5}$ concentrations downwind of the dairy ranged from 15.4 to 56.0 μg m^{-3}, with upwind levels ranging from 13.6 to 31.4 μg m^{-3}. Measured downwind PM_{10} concentrations ranged from 59.2 to 138.6 μg m^{-3}, and upwind PM_{10} levels ranged from 42.3 to 104.5 μg m^{-3}. Measured TSP concentrations downwind of the dairy ranged from 129.9 to 246.4 μg m^{-3}, with upwind levels ranging from 69.8 to 188.4 μg m^{-3}. In general, the highest downwind concentrations of all mass size fractions were measured at 2 m above ground level, with elevated measurements at 5 m and 9 m reporting slightly lower values. This same decreasing concentration with increasing measurement height trend was observed in OPC measurements. Figure 5 shows the correlation between upwind and downwind MiniVol measurements. The vertical axis shows the concentrations measured at locations D, AQ, and E in figure 1 over all seven sampling periods, whereas the horizontal axis shows the concentrations measured at location A during the same periods.

MCF values were estimated for each of the MiniVol sample periods using data from sampler clusters that had both an OPC and MiniVols. Because the MCF can only be calculated during time periods when both the OPCs and MiniVols are operating, emission rates can only be determined from the lidar data during the filter sampler operational periods. Furthermore, as mentioned above, it was observed that the OPC-measured PSD of the atmospheric aerosol changed over the course of the day. However, the MiniVol sample period determines the time period over which the MCF is calculated. As a result, it was necessary to treat the calculated MCF as though it were the correct value "on average," even though the true MCF value may have varied over the time period of the measurement. Average MCFs for each sample period were calculated as the sum of the measured mass concentration values divided by the sum of the measured volume concentration values across all sample clusters and are shown in table 1, along with the average of all seven periods ±95% confidence intervals. The measured values of $MCF_{2.5}$ on June 13 and 20 were twice as high as on the other days. The measurement periods of those two days were both in the latter half the day, as previously described. Sample period mean temperatures were higher and mean relative humidities were lower than for other samples, as would be expected for the noon-to-midnight hours compared to midnight-to-midnight hours. Another significant difference observed during these two sample periods over the others was that the wind blew consistently out of the west for several consecutive hours, which may have changed the composition and size distribution of the background aerosol due to different upwind sources. Variability of the MCF of similar magnitude has been observed on other field campaigns (Williams et al., 2010).

Aglite Measurements

The Aglite lidar was placed approximately 800 m due west of the southwest corner of the dairy. It was run continuously from noon on June 13 until 19:30 on June 19, at which time the laser malfunctioned and prevented further measurements. The instrument ran in a continuous repeating scan pattern, as described above. The post-processing data conversion to aerosol concentration profiles was accomplished as previously detailed. As verification of the quality of the lidar data, the PM concentrations measured by Aglite at 10 m above ground level (the lower limit of Aglite scan height near the point sensor locations) were found to be

Table 1. Average calculated mass conversion factors (±95% CI) for each measurement period.

MCF	June 13	June 14	June 15	June 16	June 17	June 18	June 20	Average
Duration (h)	11	22.5	22.5	22.5	22.5	11.5	12	--
$PM_{2.5}/V_{2.5}$	5.56	2.71	2.67	2.03	1.89	1.96	4.83	3.09 ±1.10
PM_{10}/V_{10}	1.43	1.28	1.27	1.24	1.13	1.17	1.58	1.30 ±0.12
TSP/V_{TSP}	0.90	0.90	0.94	0.85	0.87	0.89	1.29	0.95 ±0.11

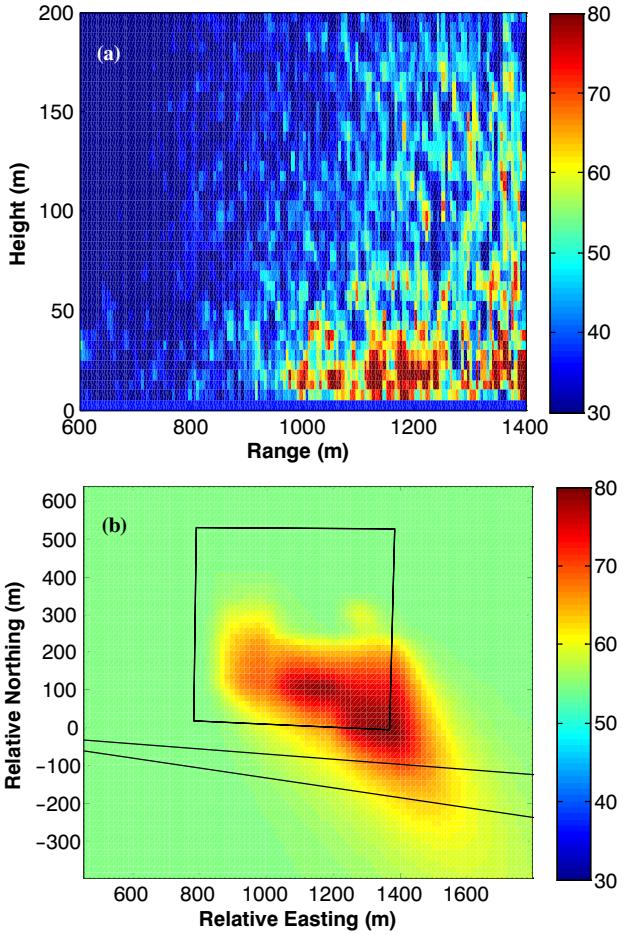

Figure 6. (a) Average PM_{10} concentration (µg m^{-3}) of all vertical scans measured by lidar at both 94˚ and 98˚ azimuth and (b) horizontal average PM_{10} concentration map estimated by AERMOD overlaid on the dairy footprint, for the first 6 h of the sampling period on June 13.

consistent with those measured by the downwind point sensor instruments (mounted at 2, 5, and 9 m heights) during all measurement periods. Figure 6a is the average downwind vertical profile of the PM_{10} concentration as measured by Aglite of the first 6 h of the sampling period on June 13, from 12:00 to 18:00. Shortly after 18:00 h, the wind direction shifted to coming from due west, hampering the effectiveness of the instrument placement. Figure 6b is the corresponding horizontal concentration map of period-average PM_{10} concentrations as predicted using inverse modeling with AERMOD at a 10 m height added to the period average background of 54 µg m^{-3}. The figure also shows the downwind profile lidar beam paths (dotted lines) used to construct figure 6a and the footprint of the dairy. It should be noted that the lidar was unable to scan past a range of 1400 m due to obstruction by power lines running along the east boundary of the dairy.

The range of maximum average concentrations in figure 6a matches somewhat with the location of maximum modeled aerosol concentration in figure 6b. Unfortunately, no point sensors were placed anywhere along the east boundary of the dairy, except for the southeast corner (location F in fig. 1). More thorough coverage of the dairy perimeter by point sensors would have either confirmed the magnitude of the concentration seen east of the dairy in figure 6b or constrained the inverse model so as to give a more accurate estimation of the plume concentration in that area. In either case, better point sensor coverage would have resulted in increased confidence in the inverse modeling results.

Calculated Emission Rates

The size-fractionated PM emission rates of the dairy were estimated for each measurement period using both inverse modeling coupled with the MiniVol sampler measurements and by application of a mass balance approach to the mass-calibrated lidar measurements, as described previously in the Methodology section. A total of 161 filter samples were taken over the course of the campaign; however, 12 of them with noted problems (dropped filter, sampler malfunction, insect on filter, etc.) were removed from further calculations. There were 109 considered downwind measurements in the remaining 149. From these 109, 91 passed the screening criteria of having a level greater than the mean upwind concentration plus the 67% confidence interval and were used in emission rate calculations, broken down by size fraction as follows: 31 $PM_{2.5}$, 41 PM_{10}, and 19 TSP. Of the 2,045 total downwind lidar scans taken throughout the whole campaign, 518 scans with identified problems were removed from emission rate calculations, mostly for the reason of excessive wind direction deviation.

The calculated emission values per sample period from inverse modeling and the average lidar measured emission rates ±95% confidence intervals are tabulated in table 2. The overall averages, standard deviations (SD), and 95% confidence intervals for each size fraction are shown at the

Table 2. Emission rates estimated using inverse modeling (IM) and lidar measurements for each sample period, as well as the average temperature and wind velocity.

Sample Date (2008)	Emission Rates ±95% Confidence Interval (g d^{-1} AU^{-1})						No. of Lidar Samples	Meteorological Conditions		
	$PM_{2.5}$		PM_{10}		TSP			Temp. (°C)	Wind Speed at 10 m (m s^{-1})	Wind Dir. (degrees)
	IM	Lidar	IM	Lidar	IM	Lidar				
June 13	13.0	2.7 ±0.9	43.5	19.0 ±6.3	100.2	58.9 ±19.6	186	33.0	2.9	307
June 14	2.3	1.6 ±0.5	21.3	19.0 ±5.4	82.1	54.1 ±15.4	392	27.2	2.4	301
June 15	1.6	0.3 ±0.2	12.7	4.0 ±3.4	48.6	12.4 ±10.5	351	27.1	2.3	321
June 16	1.7	0.8 ±0.5	16.3	14.9 ±8.7	79.7	45.0 ±26.3	331	26.7	2.6	320
June 17	1.0	1.6 ±0.6	11.9	27.2 ±10.1	39.9	88.7 ±32.9	206	25.4	3.1	313
June 18	1.3	0.6 ±0.3	7.7	6.3 ±3.7	23.7	19.1 ±11.1	61	21.9	2.1	332
June 20	5.7	--	60.4	--	157.2	--	--	34.8	1.4	306
Mean	3.8	1.3	24.8	15.1	75.9	46.4		28.8	2.5	316
SD	4.4	0.8	19.6	7.9	44.8	25.5		4.6	0.5	11
95% CI	3.2	0.2	14.5	2.2	33.2	7.0		3.2	0.3	8

Table 3. Emission rates estimated by inverse modeling and lidar measurements in this study, as well as those reported by previous studies (all values are in g d^{-1} $animal^{-1}$).

Emission	This Study		USDA (2000)	Schmidt et al. (2006)	Goodrich et al. (2006)	Martin et al. (2006)
	Inverse Modeling	Lidar				
$PM_{2.5}$	4.7 ±4.0	1.6 ±0.2	--	--	--	2.3
PM_{10}	30.7 ±18.0	18.7 ±2.7	1.8	1.7/0.3 (winter/summer)	5/15 (free-stall/open-lot)	9.2
TSP	94.0 ±41.1	57.5 ±8.7	--	--	--	--

bottom of table 2. The mean determined emission rates from both techniques were of similar magnitude.

There was significant variation in the estimated emission rates within the same technique for the different measurement periods throughout the study. In particular, inspection of table 2 shows that the PM_{10} emission rate estimated by inverse modeling was more than twice as high on June 13 and 20 than on any other day. As mentioned previously, the sampling period for those two dates covered only the afternoon and late evening, during which time it might be expected that convection is stronger than during the night and morning and more able to transport PM away from the dairy. Time-resolved lidar data show a diurnal pattern of PM emissions, with lower emissions during the morning hours and higher emissions during the afternoon hours.

The overall mean emission rates estimated by lidar and inverse modeling with ±95% confidence intervals are shown in units of g d^{-1} AU^{-1} in table 2 and in units of g d^{-1} $animal^{-1}$ in table 3. For comparison, Table 3 also shows the estimated emission values from previous studies (USDA, 2000; Schmidt et al., 2002; Goodrich et al., 2006; Martin et al., 2006).

While the overall mean PM_{10} and TSP values, as estimated by the two techniques, differed by about 40%, day-to-day differences between the two were observed, such as on June 15, when the PM_{10} emission rate estimated by the inverse modeling technique was over three times higher than the emission rate estimated by the lidar method. One factor in this may be that the two methods operate on different principles. Furthermore, inverse modeling does not simulate elevated plumes very well (Williams et al., 2010), and the lidar was unable to sample plumes lower than about 10 m off the ground due to safety and data quality concerns. These factors might explain some of the differences observed in the estimated daily average and campaign average emission rates.

The results of this study differ from those of Schmidt et al. (2002) and Martin et al. (2006) in climatic conditions and/or housing type. Goodrich et al. (2006) reported similar emissions for open-lot pens during the summer in the Texas panhandle, and lower values from free-stall areas. While Goodrich et al. (2006) also used an inverse modeling technique, the model employed was ISCST3, whereas AERMOD was used in this study. Differences of maximum predicted concentrations from ISCST3 and AERMOD of up to a factor of 2 were reported by Faulkner et al. (2008) from a ground-level area source with identical source, receptor, and meteorological inputs. This difference would be carried into inverse modeling emission rate calculations. AERMOD replaced ISCST3 as the EPA-recommended air dispersion model for regulatory purposes in December 2006. Meteorology, soil type, soil moisture, housing type, bedding type, feed, manure handling and storage, associated vehicular traffic, and animal age and activity may all be significant factors affecting PM emissions from a dairy. Based on the multiple potential factors affecting the quantification of emissions from dairies, the variation seen in the literature and herein reported are not unexpected.

CONCLUSION

This measurement campaign represents the first time that lidar has been used to estimate $PM_{2.5}$, PM_{10}, and TSP emission rates from a dairy. Estimation of facility aerosol emission rates using the lidar technique has been previously demonstrated at other agricultural facilities, including cotton gin and almond harvest operations, and its application to estimating emissions from a dairy represents a logical evolutionary advance.

Lidar measures aerosol concentration with higher spatial and temporal detail than is available from typical point-sensor-only inverse modeling approaches. Additionally, it has the ability to sense aerosols in locations that are difficult to access with point sensors, such as several hundred meters above the ground, and the ability to generate images of aerosol concentration over large areas for diagnostic purposes.

It should be noted that the emissions reported herein are not representative of the emissions throughout the year, as measurements were taken under summer conditions (hot and dry) with relatively dry soil, and emissions during other seasons are expected to be lower due to emission suppression from precipitation events, among other factors. In order to determine suitable values for regulatory purposes, surveys of particulate emission rates should made at a variety of different dairies and pen types during different times of the year.

These kinds of measurements can be used to evaluate different management scenarios in order to understand and minimize the environmental impacts of commercial dairies, as well as other types of agricultural facilities. The results of the experiment described here indicate that it is technically feasible to use the techniques described here for such purposes. It is expected that improved lidar hardware designs in the future will increase the quality of the results from the lidar technique by increasing both the number and the quality of individual lidar scans taken in a measurement period. Furthermore, the quality of the inverse modeling results could be improved through the use of larger numbers of point sensors, distributed so as to cover more of the facility perimeter.

Because of its technical complexity and high cost, the lidar measurement technique may be financially impractical for monitoring massive numbers of individual facilities. Nevertheless, the mass balance technique of lidar for estimating the net emission rate is fundamentally different

from inverse modeling, meaning that lidar offers a way to validate the inverse modeling technique. Furthermore, lidar is potentially able to estimate the emission rate with much higher temporal and spatial resolution than inverse modeling, meaning that it may be used to quantify the efficacy of management practices. A possible future scenario for PM emissions monitoring may involve using lidar to compare various management practices and to validate cheaper techniques for monitoring individual facility compliance.

REFERENCES

Baldauf, R. W., D. D. Lane, G. A. Marotz, and R. W. Wiener. 2001. Performance evaluation of the portable MiniVOL particulate matter sampler. *Atmos. Environ.* 35(35): 6087-6091.

Bingham, G. E., C. C. Marchant, V. V. Zavyalov, D. J. Ahlstrom, K. D. Moore, D. S. Jones, T. D. Wilkerson, L. E. Hipps, R. S. Martin, J. L. Hatfield, J. H. Prueger, and R. L. Pfeiffer. 2009. Lidar-based emissions measurement at the whole-facility scale: Method and error analysis. *J. Appl. Remote Sens.* 3: Paper No. 033510.

Chen, F. L., R. Williams, E. Svedsen, K. Yeatts, J. Creason, J. Scott, D. Terrell, and M. Case. 2007. Coarse particulate matter concentrations from residential outdoor sites associated with the North Carolina Asthma and Children's Environment Studies (NC-ACES). *Atmos. Environ.* 41(6): 1200-1208.

Chow, J. C., J. G. Watson, S. A. Edgerton, E. Vega, and E. Ortiz. 2002. Spatial differences in outdoor PM_{10} mass and aerosol composition in Mexico City. *J. Air Waste Mgmt.* 52(4): 423-434.

Cooper, D. I., W. E. Eichinger, D. E. Hof, D. Seville-Jones, R. C. Quick, and J. Tiee. 1994. Observations of coherent structures from a scanning lidar over an irrigated orchard. *Agric. Forest Meteorol.* 67(3-4): 239-252.

Cowherd, C. 2005. Chapter 28: Fugitive dust emissions. In *Aerosol Measurement: Principles, Techniques, and Applications*, 845-858. 2nd ed. P. A. Baron and K. Willeke, eds. Hoboken, N.J.: John Wiley and Sons.

Dias, J. M. B., J. M. N. Leitão, and E. S. R. Fonseca. 2004. Reconstruction of backscatter and extinction coefficients in lidar: A stochastic filtering approach. *IEEE Trans. Geosci. Remote Sensing* 42(2): 443-456.

Eichinger, W. E., H. E. Hoder, D. I. Cooper, L. E. Hipps, R. Knight, W. P. Kustas, J. Nichols, and J. H. Prueger. 2005. Lidar measurement of boundary layer evolution to determine sensible heat fluxes. *J. Hydrometeorol.* 6(6): 941-953.

EPA. 1987. 40 CFR Appendix J to Part 50: Reference method for the determination of particulate matter as PM_{10} in the atmosphere. *Federal Register* 54: 24664. Washington, D.C.: U.S. Environmental Protection Agency.

EPA. 2004. 40 CFR 50.7: National primary and secondary ambient air quality standards for $PM_{2.5}$. *Federal Register* 69: 45595. Washington, D.C.: U.S. Environmental Protection Agency.

EPA. 2006. 40 CFR 50.6: National primary and secondary ambient air quality standards for PM_{10}. *Federal Register* 71: 61224. Washington, D.C.: U.S. Environmental Protection Agency.

EPA. 2008. 40 CFR 122.23. Concentrated animal feeding operations. *Federal Register* 73: 70480. Washington, D.C.: U.S. Environmental Protection Agency.

Faulkner, W. B., B. W. Shaw, and T. Grosch. 2008. Sensitivity of two dispersion models (AERMOD and ISCST3) to input parameters for a rural ground-level area source. *J. Air Waste Mgmt.* 58(10): 1288-1296.

Goodrich, L. B., C. B. Parnell, S. Mukhtar, and S. C. Capereda. 2006. A PM_{10} emission factor for free-stall dairies. In *Proc. Workshop on Agricultural Air Quality: State of the Science*, 628-629. V. P. Aneja et al., eds. Raleigh, N.C.: North Carolina State University.

Hansen, F. V. 1993. Albedos. ARL-TR-57. Adelphi, Md.: U.S. Army Research Laboratory.

Hess, M., P. Koepke, and I. Schult. 1998. Optical properties of aerosols and clouds: The software package OPAC. *Bull. American Meteorol. Soc.* 79(5): 831-844.

Hiscox, A. L., D. R. Miller, B. A. Holmén, W. Yang, and J. Wang. 2008. Near-field dust exposure from cotton field tilling and harvesting. *J. Environ. Qual.* 37(2): 551-556.

Holmén, B. A., W. E. Eichinger, and R. G. Flocchini. 1998. Application of elastic lidar to PM_{10} emissions from agricultural nonpoint sources. *Environ. Sci. Tech.* 32(20): 3068-3076.

Holmén, B. A., T. A. James, L. L. Ashbaugh, and R. G. Flocchini. 2001. Lidar-assisted measurement of PM_{10} emissions from agricultural tilling in California's San Joaquin Valley: Part I. Lidar. *Atmos. Environ.* 35(19): 3265-3277.

Holmén, B. A., D. R. Miller, A. L. Hiscox, W. Yang, J. Wang, T. Sammis, and R. Bottoms. 2008. Near-source particulate emissions and plume dynamics from agricultural field operations. *J. Atmos. Chem.* 59(20): 117-134.

Jursa, A. S. 1985. *Handbook of Geophysics and the Space Environment*. Hanscom Air Force Base, Mass.: U.S. Air Force Geophysics Laboratory.

Lange, J. M., R. E. Lacey, C. B. Parnell Jr., and W. D. James. 2009. Crustal fraction of cattle feedlot particulate matter emissions using neutron activation analysis: Method development. *J. Radioanal. Nuclear Chem.* 281(2): 253-257.

Ma, X., J. Q. Lu, R. S. Brock, K. M. Jacobs, P. Yang, and X.-H. Hu. 2003. Determination of complex refractive index of polystyrene microspheres from 370 to 1610 nm. *Phys. Med. Biol.* 48(24): 4165-4172.

Marchant, C. C., T. D. Wilkerson, G. E. Bingham, V. V. Zavyalov, J. M. Andersen, C. B. Wright, S. S. Cornelsen, R. S. Martin, P. J. Silva, and J. L. Hatfield. 2009. Aglite lidar: A portable elastic lidar system for investigating aerosol and wind motions at or around agricultural production facilities. *J. Atmos. Remote Sens.* 3(1): 033511.

Marchant, C. C., M. D. Wojcik, and W. J. Bradford. 2011. Estimation of aerosol effective radius by multi-wavelength elastic lidar. *IEEE Trans. Geosci. Remote Sensing* (in press).

Martin, R. S., K. D. Moore, and V. S. Doshi. 2006. Unpublished data. Logan, Utah: Utah State University.

Measures, R. M. 1984. *Laser Remote Sensing: Fundamentals and Applications.* New York, N.Y.: John Wiley and Sons.

Oke, T. R. 1987. *Boundary Layer Climates.* London, U.K.: Methuen.

Schmidt, D. R., L. D. Jacobsen, and K. A. Janni. 2002. Continuous monitoring of ammonia, hydrogen sulfide, and dust emissions from swine, dairy, and poultry barns. ASAE Paper No. 024060. St. Joseph, Mich.: ASAE.

Stoughton, T. E., D. R. Miller, X. Yang, and K. M. Ducharme. 1997. A comparison of spray drift predictions to lidar data. *Agric. Forest Meteorol.* 88(1-4): 15-26.

USDA. 2000. Air quality research and technology transfer programs for concentrated animal feeding operations. Washington, D.C.: USDA Agricultural Air Quality Task Force.

Williams, D. J., S. Chilingaryan, and J. Hatfield. 2010. Measurements of particulate matter emissions from agricultural operations utilizing elastic lidar from the Los Banos tillage experiment. Washington, D.C.: U.S. Environmental Protection Agency.

Zavyalov, V. V., C. C. Marchant, G. E. Bingham, T. D. Wilkerson, J. L. Hatfield, R. S. Martin, P. J. Silva, K. D. Moore, J. Swasey, D. J. Ahlstrom, and T. L. Jones. 2009. Aglite lidar: Calibration and retrievals of well characterized aerosols from agricultural operations using a three-wavelength elastic lidar. *J. Appl. Remote Sens.* 3(1): 033522.